Transactions of the TSME (2014) Vol. 2, No. 2, 111~121
Journal of Research and Applications in Mechanical Engineering

ISSN 2229-2152 print
DOI: 10.14456/jrame.2014.12

Research Article

INVESTIGATION OF SWIRLING FLOW-FIELD IN AN ISOTHERMAL VORTEXING FLUIDIZED BED COMBUSTOR

S. Sripattanapipat*
Faculty of Engineering, Mahanakorn University of Technology, Bangkok 10530, Thailand

ABSTRACT:
A two-dimensional mathematical model of strongly swirling turbulence flow in the vortexing fluidized bed combustor (VFBC) is performed in this paper. Computations, based on finite volume method, were carried out by utilizing the standard k-ε model and the Algebraic Reynolds stress model (ASM) for the closure of the second-order correlation moment in the time averaged governing equations. It is observed that the Algebraic Reynolds stress model (ASM) performs better than the k-ε model in predicting the axial and tangential velocity profiles. In addition, computations using different numerical differencing schemes found that the use of upwind and hybrid schemes leads to slightly better results than that of QUICK and SOU schemes.

Keywords: *Vortexing fluidized bed combustor (VFBC), swirling flow*

1. INTRODUCTION

A vortexing fluidized bed combustor (VFBC) was developed and investigated by Soward [1] to increase the residence time of solid fuel particles in the freeboard, to reduce loss of fine particles from the combustor, and to abate the pollutants. VFBC has been of considerable interest over the past decades because of their occurrence in industrial applications. It consisted of a swirl/vortex generating system which was formed by injecting secondary air tangentially into the freeboard. The mathematical models including the turbulence models, numerical solution and other computational details are described. Comparisons of the calculated gas tangential and axial velocities with the test data measured in an isothermal flow vortexing fluidized-bed combustor of Lin et al. [2] are made to evaluate the turbulence models used. This investigation aimed to expand the technical database, have a better understanding of the involved physical processes, and guide the design and operation of the VFBC. Blaszczuk et al. [3] presented the mass balance model to predict operating conditions of coal-fired circulating fluidized bed (CFB) combustor under full load operation which was developed for the particle size distribution and solids mass fluxes of three granular materials supplied and led out in the 966 MWth supercritical circulating fluidized bed boiler. The model can theoretically predict the PSD and mass balance at different operating loads, ash content and points inside the supercritical CFB combustion system. Zhang et al. [4] conducted the comprehensive numerical modelling of the strongly swirling gas-particle turbulent flow and pulverized coal combustion in a novel vortex combustor recently developed for commercial heating applications. The numerical results for an 88 kW coal fired vortex combustor describe the detailed characteristics of the gas-particle flow and combustion in terms of gas velocities, turbulence quantities, temperature, species concentrations, particle density, trajectories, burnout time and residence time.

* Corresponding author: S. Sripattanapipat
E-mail address: ssomchai@mut.ac.th

Ridluan et al. [5] conducted the numerical simulations of strongly swirling turbulent flows in a vortex combustor (VC) by using three first-order turbulence models: the standard k–ε turbulence model, Renormalized Group (RNG) k-ε model and shear stress transport (SST) k-ω model; and a second-order turbulence model, Reynolds stress model (RSM) together with a second-order numerical differencing schemes. Axial and tangential velocities, pressure fields, and turbulence kinetic energy characteristics were also investigated. Their results indicated that RSM was superior to other turbulence models in capturing the swirl flow effect. Ezhil Kumar et al. [6] analyzed the reacting and non-reacting flow structure in a three dimensional trapped vortex combustor (TVC) cavity by using shear stress transport (SST) k-ω, k-ω model and eddy dissipation combustion model. They found that fuel-air mixing was considerably improved as momentum flux ratio (MFR) increased. However, the secondary jet showed insignificant effect on cavity flow structure. Merlin et al. [7] studied the flow and flame dynamics inside a trapped vortex combustor at various main flow rates and lengths of the cavity by using Large Eddy simulation. Their results suggested that swirling motion was mandatory to favor the global burner stability.

The primary aim of this research is to investigate numerically the swirling flow in an isothermal vortexing fluidized bed combustor (VFBC) in order to have a better understanding of flow behaviors. Numerical computations were performed using the standard k-ε turbulence model and Algebraic Reynolds stress model (ASM) together with the numerical differencing schemes (upwind, hybrid, QUICK and SOU schemes) for prediction. The numerical results are validated with the available experimental data [2].

2. MATHEMATICAL MODELING AND SOLUTION PROCEDURE

The phenomenon under consideration is governed by the steady two-dimensional form of the continuity and the time-averaged incompressible Navier-Stokes equations. In the Cartesian tensor system these equations can be written in the following form:

$$\frac{\partial}{\partial x_i}\left(\rho u_i\right) = 0 \tag{1}$$

$$\frac{\partial(\rho u_i u_j)}{\partial x_j} = -\frac{\partial p}{\partial x_i} + \frac{\partial}{\partial x_j}\left(\overline{t}_{ij} + \tau_{ij}\right) S_{ut} \tag{2}$$

where ρ, u_i, p and x_i are the density, mean velocity tensor, mean pressure and coordinate tensor respectively. The mean viscous stress tensor, $\overline{t}_{ij}$ is approximated as:

$$\overline{t}_{ij} = \mu\left(\frac{\partial u_i}{\partial x_j} + \frac{\partial u_j}{\partial x_i}\right) \tag{3}$$

where μ is laminar viscosity, the time-averaged Reynolds stress tensor, $\tau_{ij} = -\rho\overline{u_i' u_j'}$, in the above equation is not known and thus, models are needed to express it in terms of the solution variables. In the present study, two turbulence models are used, namely the k-ε model and an algebraic stress model (ASM). The standard k-ε model version relates the turbulent eddy viscosity to the turbulence kinetic energy, k and the dissipation rate, ε through Boussinesq's approximation as:

$$\tau_{ij} = -\frac{2}{3}\delta_{ij}\left(\rho k\right) + \mu_t\left(\frac{\partial u_i}{\partial x_j} + \frac{\partial u_j}{\partial x_i}\right) \tag{4}$$

where $\mu_t = \rho C_\mu k^2/\varepsilon$ is the turbulent eddy viscosity and ε is the dissipation rate of turbulence kinetic energy (TKE). The modelled equation of the TKE, k is given by:

$$\frac{\partial}{\partial x_j}\left(\rho u_j k\right)=\frac{\partial}{\partial x_j}\left(\frac{\mu_e}{\sigma_k}\frac{\partial k}{\partial x_j}\right)+G-\rho\varepsilon \tag{5}$$

in which $\mu_e = \mu_t + \mu$ is effective viscosity. Similarly the dissipation rate of TKE is given by the following equation:

$$\frac{\partial}{\partial x_j}\left(\rho u_j \varepsilon\right)=\frac{\partial}{\partial x_j}\left(\frac{\mu_e}{\sigma_\varepsilon}\frac{\partial \varepsilon}{\partial x_j}\right)+\frac{\varepsilon}{k}\left(C_{\varepsilon 1}G-C_{\varepsilon 2}\rho\varepsilon\right) \tag{6}$$

where G is the rate of generation of the TKE while $\rho\varepsilon$ is its destruction rate. G is given by:

$$G=\mu_e\left[\left(\frac{\partial u_i}{\partial x_j}+\frac{\partial u_j}{\partial x_i}\right)\frac{\partial u_i}{\partial x_j}\right] \tag{7}$$

The boundary values for the turbulent quantities near the wall are specified with the wall function method. C_μ = 0.09, $C_{\varepsilon 1}$ = 1.44, $C_{\varepsilon 2}$ = 1.92, σ_k = 1.0, and σ_ε = 1.3 are empirical constants in the turbulence transport equations. Reynolds-averaged transport equations can be solved for τ_{ij}, the modelled equations for which are:

$$\frac{\partial \tau_{ij}}{\partial t}+\frac{\partial(u_k\tau_{ij})}{\partial x_k}=-G_{ij}-\Phi_{ij}+D_{ij}+\varepsilon_{ij} \tag{8}$$

where

$$G_{ij}=\text{local production}=\rho P_{ij}=-\left(\rho\overline{u_i'u_k'}\frac{\partial u_j}{\partial x_k}+\rho\overline{u_j'u_k'}\frac{\partial u_i}{\partial x_k}\right)$$

$$\Phi_{ij}=\text{local pressure strain}=-C_1\frac{\rho\varepsilon}{k}\left(\overline{u_i'u_j'}-\frac{2}{3}k\delta_{ij}\right)-C_2\left(G_{ij}-\frac{2}{3}G\delta_{ij}\right)$$

$$D_{ij}=\text{net diffusive transport}=-\frac{\partial}{\partial x_k}\left(\left(\frac{\mu_e}{\sigma_T}\right)\frac{\partial\overline{u_i'u_j'}}{\partial x_k}\right)$$

$$\varepsilon_{ij}=\text{local dissipation tensor}=\frac{2}{3}\rho\varepsilon\delta_{ij}$$

in which C_1 = 2.5, and C_2 = 0.55 are model constants.

Algebraic Reynolds Stress Model (ASM): For simplicity in solving the six Reynolds stresses, Rodi's approximation is used in this study and the Reynolds stress transport can be expressed in algebraic form as follows:

$$\frac{D\tau_{ij}}{Dt}-D_{ij}=\frac{\tau_{ij}}{\rho k}\left(\frac{Dk}{Dt}-D_k\right) \tag{9}$$

Substitution of Eq. (5) and (8) into Eq. (9) gives the desired algebraic expression for τ_{ij} :

$$-G_{ij}-\Phi_{ij}+\frac{2}{3}\delta_{ij}\rho\varepsilon=\frac{\tau_{ij}}{\rho k}\left(G-\rho\varepsilon\right) \tag{10}$$

The ASM expressions can thus be rewritten as:

$$\rho\overline{u_i'u_j'} = \frac{2}{3}\delta_{ij}\rho k + \frac{\lambda k}{\varepsilon}\left(G_{ij} - \frac{2}{3}\delta_{ij}G\right) \tag{11}$$

where the empirical constant, λ was found to be 0.135, is defined as:

$$\lambda = \frac{1-C_2}{C_1 - 1 + \dfrac{G}{\rho\varepsilon}} \tag{12}$$

All the governing equations can be re-organized and expressed in a standard form that includes the convection, diffusion, and source terms for 2-D flows as follows:

$$\frac{\partial}{\partial x}(\rho u\phi) + \frac{\partial}{\partial y}(\rho v\phi) - \frac{\partial}{\partial x}\left(\Gamma_{\phi x}\frac{\partial \phi}{\partial x}\right) - \frac{\partial}{\partial y}\left(\Gamma_{\phi y}\frac{\partial \phi}{\partial y}\right) = S_\phi \tag{13}$$

where ϕ may stand for any variable including the velocity components, Γ_x and Γ_y are the exchange coefficients for ϕ, and S_ϕ is the source term.

In the present computation, the time-averaged Navier-Stokes equations, are solved numerically by a control-volume finite-difference method [8] together with the turbulence model equations. All equations are in a generalised form of equation (9). The SIMPLE algorithm is utilized for pressure-velocity de-coupling and iteration [8, 9]. The first-order upwind was used for discretising convection and diffusion transports on a staggered grid cell. The under-relaxation iterative TDMA line-by-line sweeping technique [10, 11] is used for solving the resultant finite-difference equations. The computation was carried out using a personal computer. About 20,000 iterations were needed to achieve satisfactory convergence for each calculation, requiring about 1.0 hr of computer time.

3. VORTEXING FLUIDIZED BED COMBUSTOR CONFIGURATIONS

A strongly swirling flow in VFBC of Lin et al. [2] was selected for the validation of the computational results. The schematic diagram of VFBC is shown in Fig. 1. It comprised a cylindrical chamber having a diameter (D) of 0.19 m and a height of 2.28 m (12D). The tangentially injected secondary air nozzles with a diameter (d) of 0.019 m and an exhaust tube with a diameter (D_e) 0.095 m were located at 0.57 m (3D) and 2.09 m (11D) above the bottom of chamber, respectively. A two dimensional axisymmetric coordinate system was used to describe VFBC freeboard region, as shown schematically in Fig. 1. The primary air flows from the bottom into the domain of interest for simulation. The flow mixes with the tangentially injected secondary air and leaves the domain through the exhaust tube at the top. The schematic diagram of the diameter of imaginary circle, (D_s), and the arrangement secondary air injection nozzles are shown in Fig. 2. Axial and tangential velocities were taken from eight vertical locations (x/D = 3, 4, 5, 6, 7, 8, 9, and 10) to compared with the available experimental data [2]. Unfortunately, Lin et al. [2] did not provide the experimental inlet velocities of primary and secondary air, thus these data were estimated by extrapolation using known velocity distributions upstream of the entrance. The relation of primary to secondary air flow rate ratio was used to calculate U_B, V_j and l as shown below:

$$U_B = Q_r \times \frac{4w}{D_s} \times \frac{d_0^2}{D} \tag{14}$$

$$V_j = w\frac{\sqrt{D^2 - D_s^2}}{D_s} \tag{15}$$

$$l = \frac{d_0^2}{\sqrt{D^2 - D_s^2}} \tag{16}$$

where the tangential velocity, w was estimated by extrapolation, Q_r is defined as the ratio of volumetric flow rates of primary air to the secondary air (Q_B/Q_j), U_B is the primary air velocity, V_j is the radial secondary air velocity, and

l is the size of nozzles. In the present simulation, the applied dimensions were D = 0.19 m, D_s = 0.1805 m, d_o = 0.019 m, and D_e = 0.095 m. The inlet conditions from the extrapolation of experimental data [2] are shown as follows: the tangential velocity, w = 9-15 m/s, Q_r = 1.0-2.0, D_s/D = 0.5-1.0, the primary air velocity, U_B = 0.8-1.2 m/s, the radial secondary air velocity, V_j = 4.36-25.98 m/s and the size of nozzle slot, l = 2.194-4.359 mm.

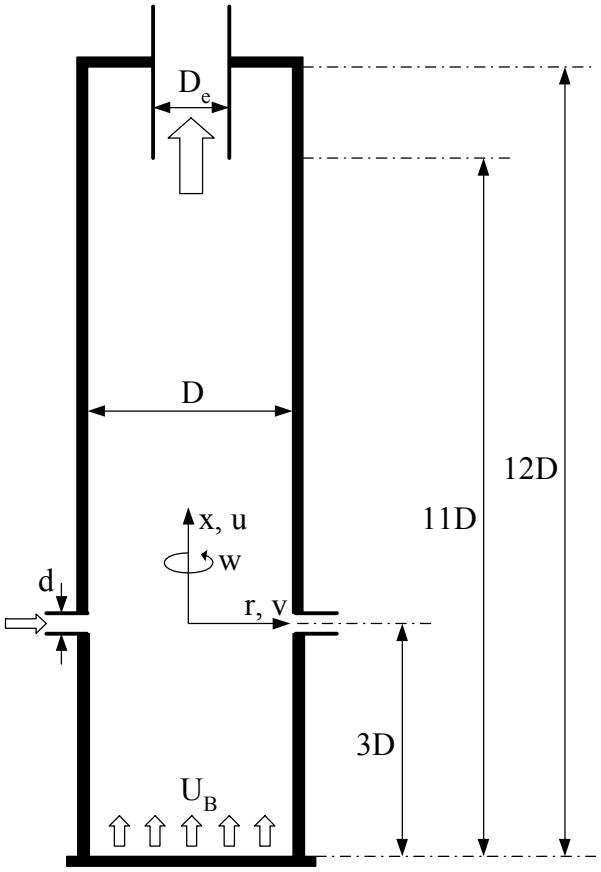

Fig. 1. Computation domain of vortexing fluidized bed combustor (VFBC).

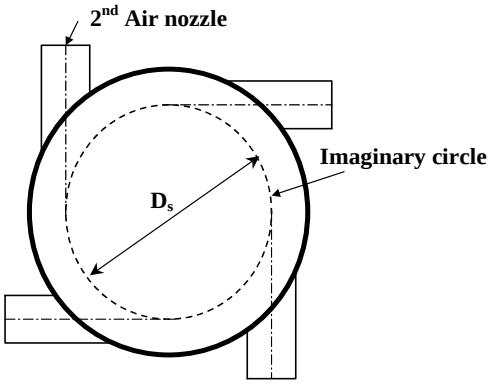

Fig. 2. The imaginary circle of injection nozzles of vortexing fluidized bed combustor (VFBC).

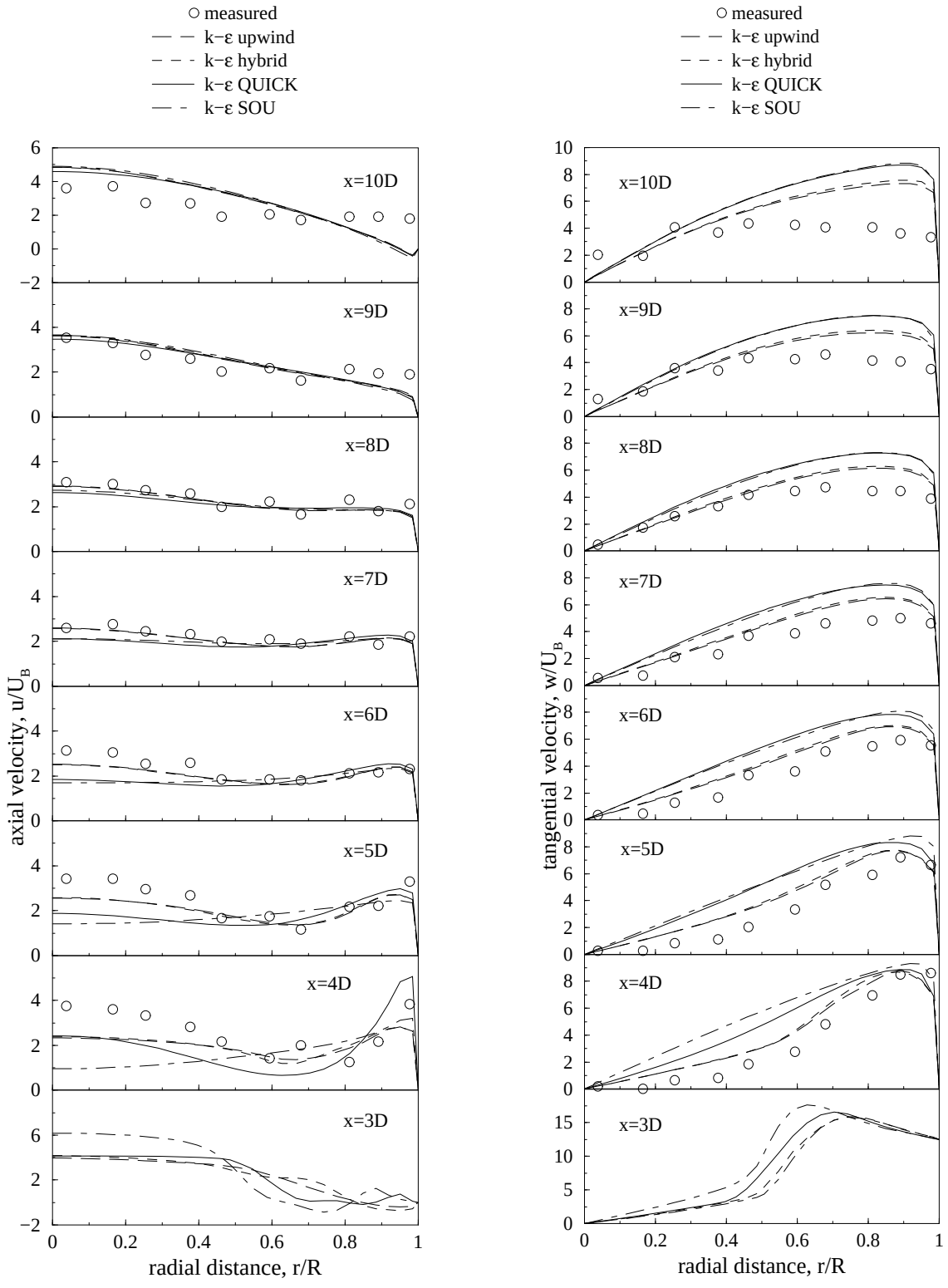

(a) axial velocity (b) tangential velocity

Fig. 3. Comparison of measurements with predictions using k-ε model at various schemes for Q_r = 1, D_s/D = 0.5, w = 15 m/s, U_B = 1.2 m/s, V_j = 25.98 m/s and l = 2.194 mm.

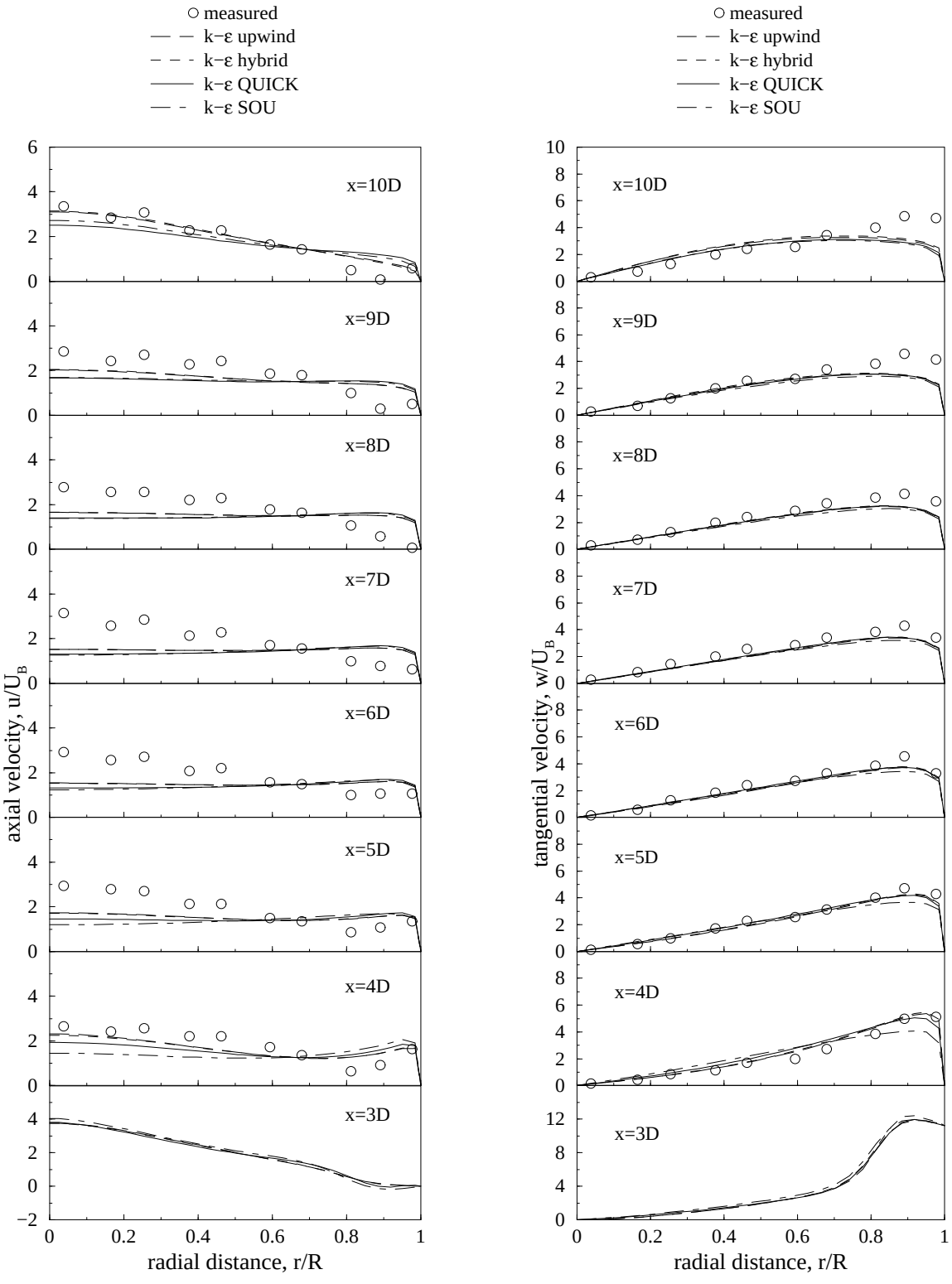

(a) axial velocity (b) tangential velocity

Fig. 4. Comparison of measurements with predictions using k-ε model at various schemes for Q_r = 2, D_s/D = 1.0, w = 9 m/s, U_B = 0.8 m/s, V_j = 4.36 m/s and l = 4.359 mm.

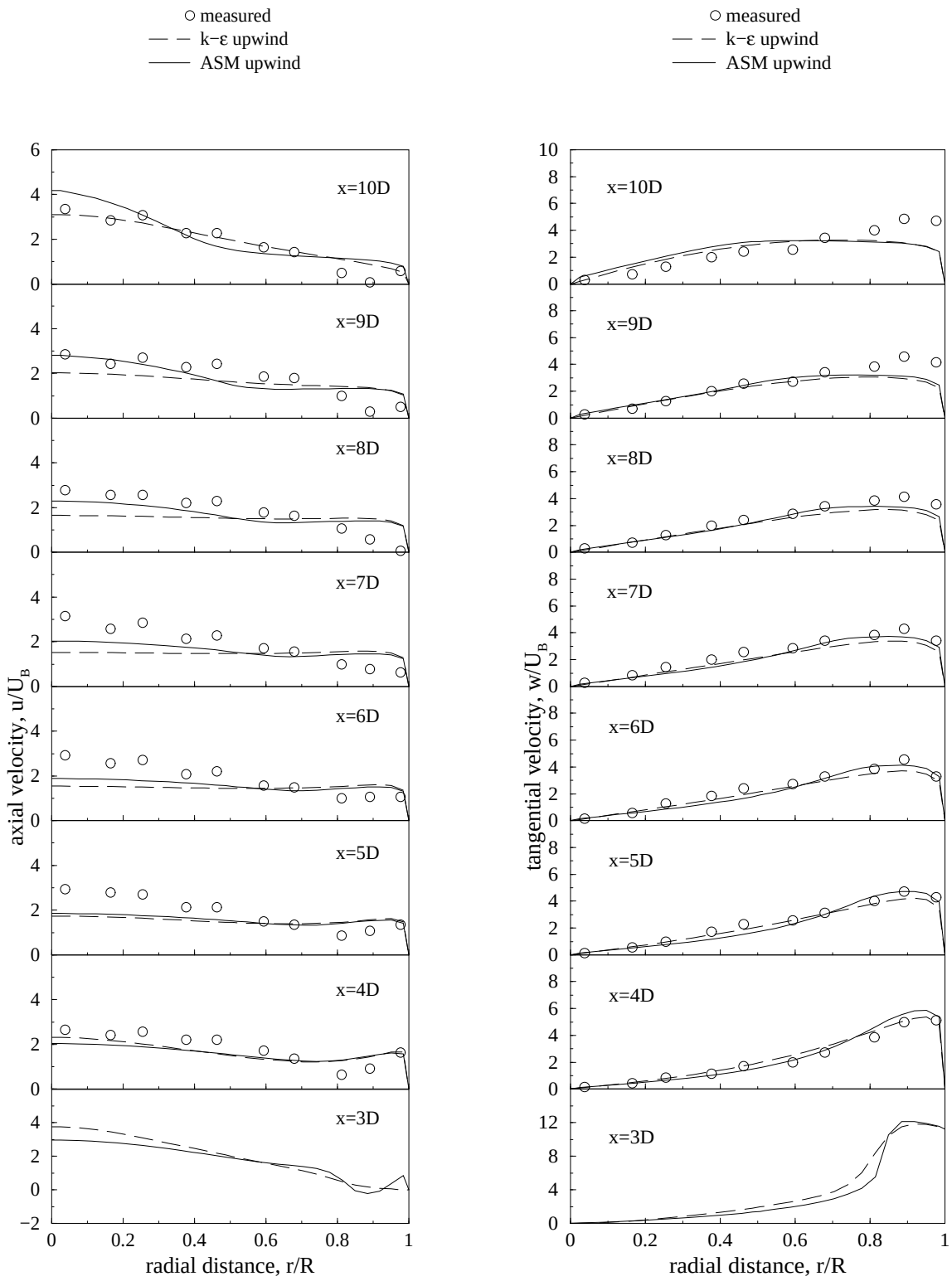

(a) axial velocity (b) tangential velocity

Fig. 5. Comparison of measurements with predictions using Algebraic Reynolds stress model (ASM) and k-ε model for Q_r = 2, D_s/D = 1.0, w = 9 m/s, U_B = 0.8 m/s, V_j = 4.36 m/s and l = 4.359 mm.

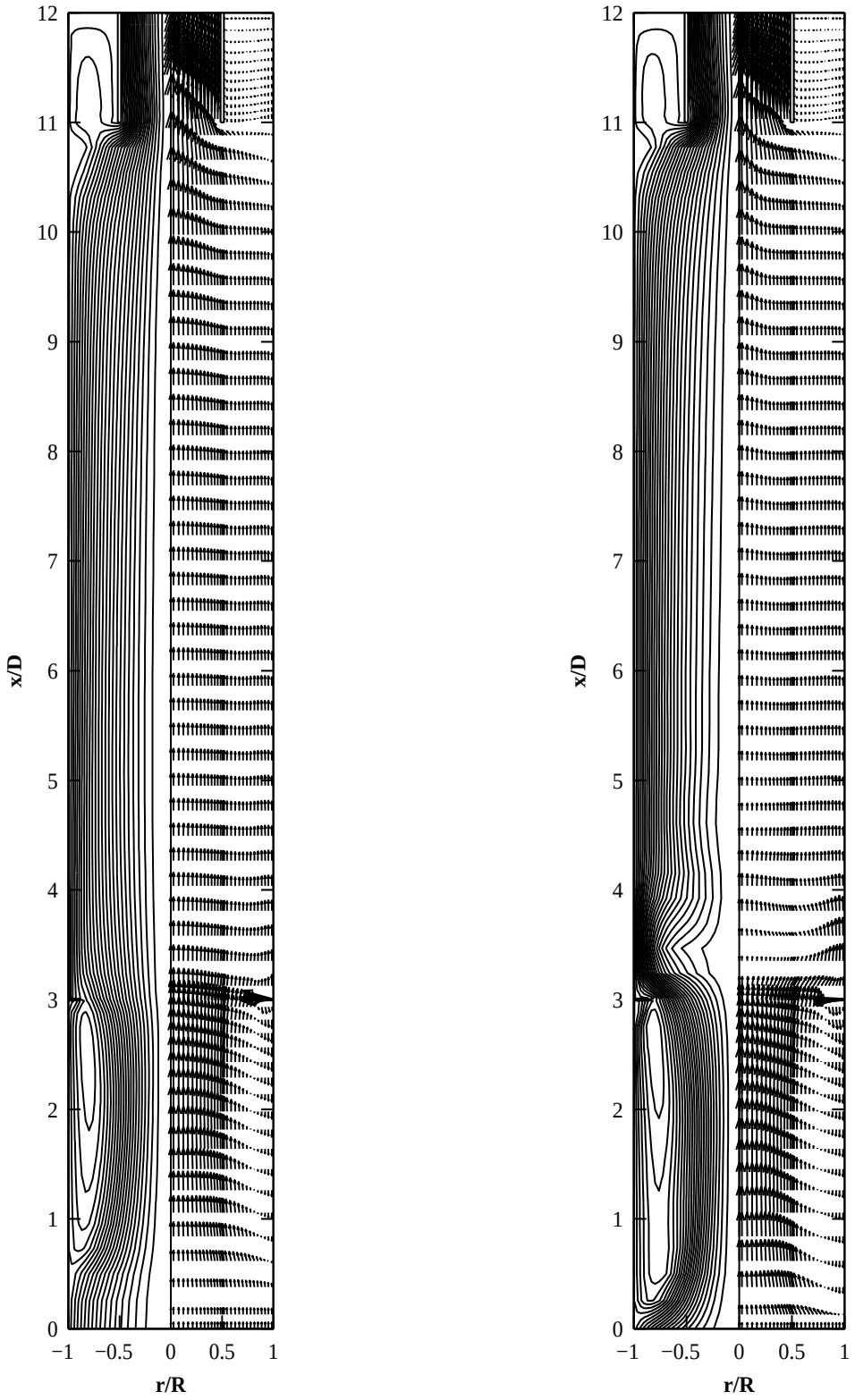

(a) upwind scheme (b) SOU scheme

Fig. 6. Streamlines and vector plot of velocities predicted by Algebraic Reynolds stress model (ASM).

4. RESULTS AND DISCUSSION

To evaluate the reliability of the present simulation, the predicted axial and tangential velocities are compared with with measured data of Lin et al., [2] as shown in Fig. 3. The normalized axial and tangential mean velocity profiles predicted using the k-ε model with four different numerical schemes are presented in Fig. 3 (for $Q_r = 1$, $D_s/D = 0.5$, $w = 15$ m/s, $U_B = 1.2$ m/s, $V_j = 25.98$ m/s, and $l = 2.194$ mm). Generally, the predicted axial and tangential velocity profiles by all numerical schemes are similar to the experimental data. Predicted axial velocities from all schemes are comparable and they are in fairly good agreement with measurements. However, tangential velocities are over predicted, especially for $5.0 \le x/D \le 10$ and $0.4 \le r/R \le 1.0$. For the studied schemes, upwind and hybrid schemes offer more accurate data than QUICK and SOU ones, particularly for tangential velocity prediction. Fig. 3 also shows that at the same vertical location, mean tangential velocities are higher than axial ones, indicating a highly swirling flow. In addition, tangential velocity increases and then decreases in radial direction due to force and free vortex effects, respectively. The peak of tangential profile is located at the turning point which is the interface between free and force vortexes.

The normalized axial and tangential mean velocity profiles predicted using the k-ε model with four different numerical schemes are compared with measured data in Fig. 4 (for $Q_r = 2$, $D_s/D = 1.0$, $w = 9$ m/s, $U_B = 0.8$ m/s, $V_j = 4.36$ m/s, and $l = 4.359$ mm). It is found that predictions with the four schemes generally are in fairly good agreement with measurements of tangential velocity. However, use of four schemes gives under-predicted results of axial velocity profiles at $4.0 \le x/D \le 9.0$ and $0.0 \le r/D \le 0.6$ but over-predicted at $0.8 \le r/D \le 1.0$. Overall, the upwind and hybrid schemes yield slightly better result than the QUICK and SOU schemes. This maybe comes from over successive interpolations between interior grid nodes of those second-order schemes while upwind and hybrid are the first-order schemes.

In Fig. 5, the predictions with the Algebraic Reynolds stress model (ASM) are in good agreement with measured data better than the k-ε model, especially $6.0 \le x/D \le 9.0$. However, both turbulence models fail to predict the axial velocity profile near the chamber wall at $8.0 \le x/D \le 10$. In Fig. 3(b), using the k-ε model and the Algebraic Reynolds stress model (ASM) results in good agreement with measured data in capturing the solid-body rotation at $4.0 \le x/D \le 9.0$. Both turbulence models show under-prediction near the chamber wall at $8.0 \le x/D \le 10$. Overall, the Algebraic Reynolds stress model (ASM) seems better than the k-ε model in prediction of both axial and tangential velocities. This is because the Algebraic Reynolds stress model (ASM) is the second-order turbulence model whereas the other is the first-order one.

Figure 6 shows streamlines and vector predicted by the upwind and SOU schemes. Apparently, the predicted results obtained from both schemes are comparable. The aerodynamic structure possesses two recirculation zones. The large one is in the lower part below the location of secondary air injection. The small one is in the upper region, in the vicinity of the exhaust tube. It can be observed that the large recirculation zone below the injection nozzle predicted by SOU scheme is larger than that by upwind scheme. According to the velocity vector plots, the large recirculation zone predicted by upwind scheme covers $0.6 \le x/D \le 3.0$ and $0.6 \le r/R \le 1.0$ while that predicted by SOU scheme covers $0.25 \le x/D \le 3.0$ and $0.55 \le r/R \le 1.0$. This indicates that the size of recirculation zone predicted by SOU scheme is slightly larger than that predicted by upwind scheme. It should be noted that it is difficult to define the exact location and size of the small recirculation zone in the upper region as its boundary is not obvious.

5. CONCLUSION

Numerical simulation has been carried out to study the flow characteristics in the isothermal vortexing fluidized bed combustor (VFBC) and to investigate the predictive capability of the k-ε turbulence model. The different numerical schemes namely, upwind, hybrid, QUICK and SOU schemes were employed. The tangential velocity is found to dominate the flow over the VFBC indicating the highly swirling flow. All numerical schemes give over predicted tangential velocity, especially for $5.0 \le x/D \le 10$ and $0.4 \le r/R \le 1.0$. For the studied schemes, upwind and hybrid schemes offer more accurate data than QUICK and SOU ones, particularly for tangential velocity prediction. Predictions using the two models indicate that Algebraic Reynolds stress model (ASM) predicts the axial velocity profile better than using the k-ε model due to higher-order turbulence model. Deviation between predicted results and experimental data probably could be attributed from two reasons. Firstly, assumption of a 2-D axisymmetric

flow is made in the present computation instead of actual 3-D flow. Secondly, lack of exact inlet data for primary and secondary air velocities and thus, extrapolated data are used instead.

REFERENCES

[1] Sowards, N.K. Low pollution incineration of solid waste, U.S. Patent No. 3,834,326, 1974.

[2] Lin, C.H., Teng, J.T., Chyang, C.S. and Hsu, C.H. A study on the swirling flow field in the freeboard of a vortexting fluidized bed combustor, JSME international Journal, Series B, Vol. 41, 1998, pp. 538-545.

[3] Blaszczuk, A., Leszczynski, J. and Nowak, W. Simulation model of the mass balance in a supercritical circulating fluidized bed combustor, Powder Technology, Vol. 246, 2013, pp. 317-326.

[4] Zhang, J. and Nieh, S. Comprehensive modelling of pulverized coal combustion in a vortex combustor, Fuel, Vol. 76, 1997, pp. 123-131.

[5] Ridluan, A., Eiamsa-ard, S. and Promvonge P. Numerical simulation of 3D turbulent isothermal flow in a vortex combustor, International Communications in Heat and Mass Transfer, Vol. 34, 2007, pp. 860-869.

[6] Ezhil Kumar, P.K. and Mishra, D.P. Numerical simulation of cavity flow structure in an axisymmetric trapped vortex combustor, Aerospace Science and Technology, Vol. 21, 2012, pp. 16-23.

[7] Merlin, C., Domingo, P. and Vervisch, L. Large Eddy Simulation of turbulent flames in a trapped vortex combustor (TVC) - A flamelet presumed-pdf closure preserving laminar flame speed, Comptes Rendus Mécanique, Vol. 340, 2012, pp. 917-932.

[8] Patankar, S.V. Numerical Heat Transfer and Fluid Flow, Hemisphere, 1980, Washington, D.C.

[9] Wilcox, C.D. Turbulent Modelling for CFD, DCW Industries, Inc., California.

[10] Versteeg, H.K. and Malalasekera, W. An Introduction to Computational Fluid Dynamics, The Finite Volume Method, Longman Group Limited, 1995, England.

[11] Launder, B.E. and Spalding D.B. The Numerical Computation of Turbulent Flows, Computer Methods in Applied Mechanics and Engineering, North-Holland publishing Company, 1974, pp. 269-289.